The JWST Infrared Scanning Shack Hartman System: A new in-process way to measure large mirrors during optical fabrication at Tinsley

Craig Kiikka[a], Daniel R. Neal[b], John Kincade[a], Robert Bernier[a], Tony Hull[a], David Chaney[c] , Steve Farrer[b], John Dixson[b], Avery Causey[b], Steve Strohl[b]
[a]Tinsley Laboratories, 4040 Lakeside Drive, Richmond, CA USA 94806;
[b]WaveFront Sciences Incorporated, 14810 Central Avenue, SE, Albuquerque, NM USA 87123
[c]Ball Aerospace & Technologies Corp., 1600 Commerce Street, Boulder, CO USA 80301

ABSTRACT

Tinsley, under JWST funding, has led the team that has developed a novel and highly versatile piece of ground support equipment for optical surface testing the JWST beryllium mirror segments during optical fabrication. The infrared Scanning Shack Hartmann System (SSHS) offers the advantage of being able to characterize mid-to-high spatial frequency structure on a mirror from early stages of fabrication when slopes may be high and surface irregular, eliminating the need for an extra polishing step before metrology. Working at 9.3um, the system will accept and measure a wide dynamic range of surface characteristics, including roll-off near the edge of the segment. Knowledge of these surface features at the early grinding stage is imperative if characteristics such as mirror edge roll-off are to be minimized. WaveFront Sciences, producer of commercial COAS™ and Columbus™ Shack Hartmann systems, has provided systems engineering and component support for the SSHS system.

The SSHS system is based around a special Long Wave Infrared (LWIR) wavefront sensor developed by WaveFront Sciences that is scanned over the mirror surface, making sub-aperture measurements. The smaller, high resolution measurements are then stitched together to provide high resolution measurement of the entire mirror surface, even though the surface is in a rough ground state.

The system leverages technology from smaller visible instrumentation produced by Wavefront Sciences, especially those for surface sub-aperture measurements of semiconductor wafers. Although the scale of the SSHS is significantly larger than previous applications, substantial commercial technology is directly applicable to the Infrared SSHS with little or no modification. Extensive use was made of existing algorithms for frame stitching and focal spot centroiding. This paper will describe the implementation of the first infrared scanning Shack Hartmann system at Tinsley to address optical fabrication optimization of the JWST Primary Mirror Segments.

Keywords: Shack Hartmann Test, Infrared, Optical Metrology, JWST Mirror Segments, Edge Roll, Frame Stitching, Wavefront Sensor, Surface Metrology

1. INTRODUCTION

The Scanning Shack Hartmann System (SSHS) is a metrology instrument for measuring JWST Primary Mirror Segments during the optical surface grinding phase. Tinsley's Computer Controlled Optical Surfacing (CCOS) process requires precision surface figure error metrology. Based upon very light weight Beryllium, Advanced Mirror Segment Demonstrator (AMSD) finishing experience,

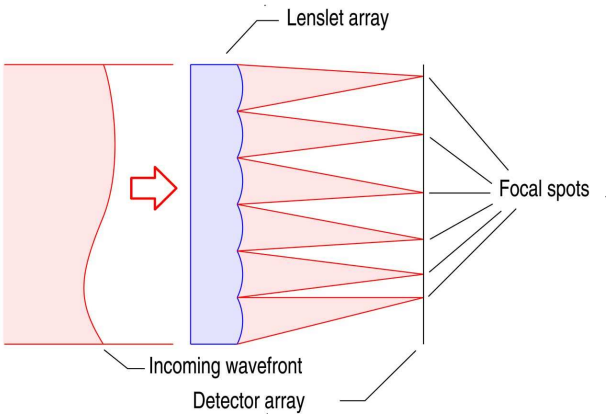

Figure 1 Basic arrangement of a Shack-Hartmann wavefront sensor.

Tinsley developed a requirement for a high spatial resolution, high surface slope error, optical, infrared, metrology instrument to complement mechanical profilometry.[12] The high density optical measurement enables faster surface figure convergence and better edge control than offered using mechanical profilometry alone. A feasibility study identified a scanning and stitching Shack-Hartmann wave front sensor as the best design concept. Wave Front Sciences, Inc. (WFSI) had developed a commercial scanning and stitching Shack-Hartmann wave front sensor, the Columbus Nanotopography system, which had already demonstrated the required precision[3] in semiconductor wafer metrology. Tinsley and WaveFront Sciences jointly completed a feasibility study and requirement flow down, culminating in a joint effort to design, fabricate, and develop this unique metrology instrument.

2. Requirements and Requirements Flow Down

The SSHS requirements flow down from the JWST Primary Mirror Segment polishing specification 579867. Per this specification, Tinsley receives ground, light-weighted substrates from Axsys Technologies and then grinds and polishes the mirror segments to a polished surface figure error specification of < 20 nm rms. The SSHS addresses the requirements for all mirror segment forms (A, B, and C). It is required to measure surface slope errors ranging from 0 – 2.2 mr, associated with the Advanced Mirror Segment Demonstrator (AMSD) experience, and is designed for surface slope errors up to 4.6 mr. The SSHS will be able to measure surfaces 0.5 – 20 μm rms. It bridges from grind to conventional optical metrology by enabling strong fringe capture at polish out. The SSHS measures mid to high spatial frequency surface figure errors, with a spatial period range from 2 mm – 222 mm. It complements precision mechanical profilometry, which provides accurate surface information for spatial periods greater than 222 mm. The shortest spatial period of 2 mm is sampled at Nyquist resolution (1 mm lenslet footprint). The SSHS provides high density data near the edge, enabling a higher degree of edge roll-off control best established in grinding. All requirements are met or improved upon by design and functionality predictions. The system requirement document identifies numerous sub tier requirements which flow into requirements for the major subsystems, the Granite Table Support and Primary Segment Mount (also used for conventional optical metrology), IR Source Assembly, Scanning Paragon Gantry subsystem, Compressor Telescope, IR Wave Front Sensor, and Reference Wave Front Subsystems.

3. SSHS Concept and Major Subsystems

The key goal of the system is to measure, at high spatial resolution and dynamic range, the entire surface of the JWST mirror segment. This is a challenging task for most any metrology system, since the desire is to measure the surface of the mirror early in the fabrication process. At this point the surface has quite a rough surface (>~1 um RMS). Hence any visible, or NIR metrology would lead to very poor results due to high optical scatter. The traditional approach of polishing the surface to get low enough roughness to allow testing in the visible would add months to the fabrication timeline. So we desired to develop a sensor that could make measurements into the LWIR. There is a combination of a CO_2 laser line with significant power, and detector sensitivity that seemed to meet these design requirements. However, an interferometer based solution would not have either sufficient resolution or dynamic range to meet the requirements developed during the AMSD experience.

The scanning Shack-Hartmann sensor concept has been extensively developed at WaveFront Sciences for silicon wafer metrology[3]. This technology is completely scalable since it relies on making sub-aperture measurements of the part and then stitching them together. Since the Shack-Hartmann sensor directly measures the wavefront slope, comparisons within the overlapped regions allows sensitive detection of alignment errors if caused by translation of the part (or sensor). Combined with the single snapshot data acquisition, stitching has been shown to work really well with a Shack-Hartmann sensor. For silicon wafer nanotopography measurements, the sensor achieves < 1 nm overall sensitivity over a 300 mm wafer, without any evident degradation caused by stitching.

Thus to meet the requirements outlined above, we conceived the idea of using a LWIR Shack-Hartmann wavefront sensor, combined with a stitching metrology system to measure the large JWST mirror segments. Instead of moving the part past a stationary sensor (as in the wafer metrology tools), we chose to fix the mirror and move the sensor. This allows accurate metrology over a very large (scalable) region at high spatial sampling density, with excellent dynamic range. In fact the dynamic range can exceed several thousands of microns, while measuring at 1 um accuracy.

Several configurations were examined, including scanning about the approximate radius of curvature and mounting the source system together with the measuring head on the gantry, before settling on testing the mirror in collimation, with a

point source at prime focus. This configuration is closest to the designed use for the mirror segment, and was therefore considered to have the lowest risk.

The SSHS consists of the following components necessary to achieve this goal:

- Long Wave Infrared Shack-Hartmann wavefront sensor (WFS) as the basic detector element to allow measurement of rough surfaces
- Relay telescope to collect light from the mirror segment and image it onto the LWIR WFS lenslet array
- Gantry to accurately scan the appropriate parts of the mirror. This included a triggering system for sending triggers to the sensor at the appropriate positions.
- CO_2 laser focused through a pinhole to act as a point source placed at the prime focus of the mirror segments
- Reference mirror system for calibrating the system in place
- Granite table and large mirror mount for positioning the elements and aligning the mirror segment

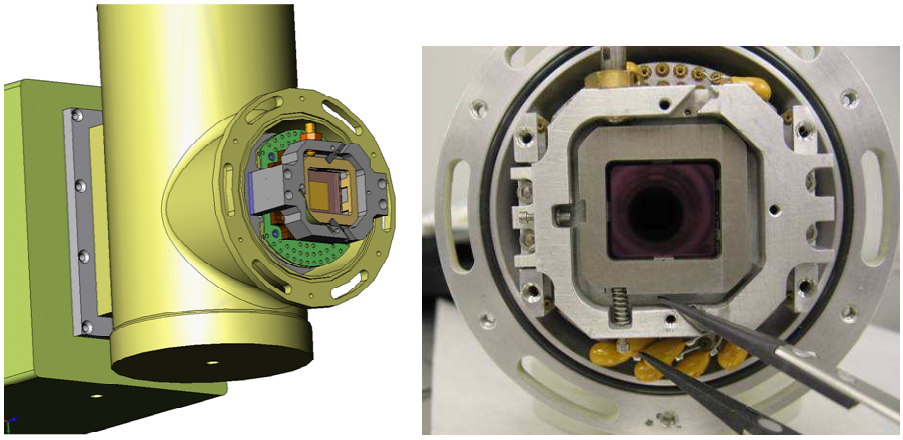

Figure 2 – Arrangement of lenslet array and detector elements in the Phoenix lab camera.

4. Long Wave Infra-Red Wave Front Sensor

1.1. Shack Hartmann wavefront sensing.

The Shack-Hartmann wavefront sensor is based on using a lenslet array to dissect the incoming wavefront distribution into a grid (or pattern) of small sections (see). The lenslet array creates a pattern of focal spots, whose motion corresponds to local variations in wavefront slope. This technology is well established for measurements in telecomm, lasers, optics, ophthalmology, manufacturing, and wafer metrology.[4,5] The sensor design, precision and accuracy, and numerous applications are all well developed, including development of NIR wavefront sensors at fairly high resolution.[6, 7, 8, 9]

1.2. Design of a LWIR WFS

The key to developing a long wavelength WFS is to identify the appropriate detector technology. We evaluated a number of different possibilities that had various advantages and disadvantages. The key problem in the LWIR is that the detector must be cooled to liquid Nitrogen (LN_2) temperatures (or below, in some cases). Thus the lenslet array either must be mounted outside of the camera window (which would require high quality IR relay imaging optics due to space constraints) or inside the vacuum dewar next to the detector focal plane array (which means that the dewar has to be accessible). Furthermore, camera resolution can significantly limit the performance of the sensor, so we desired to use cameras with at least a 640 X 480 pixel resolution. In the end we selected a modified Quantum Well Infrared Photodetector (QWIP) camera (Phoenix lab camera) manufactured by FLIR Indigo Systems in Santa Barbara. The QWIP camera operates best at about 68 K, and we achieved this by pumping on the LN_2 dewar to lower the pressure and hence the temperature. The detector was mounted in a laboratory dewar with a flanged window. This window arrangement was modified with an extension of the original cold shield to limit background radiation, and with a vacuum feed-through adjustment for the rotation of the lenslet array relative to the detector focal plane array grid. The resulting arrangement is shown in Figure 2. There were several technical challenges to overcome in designing the lenslet mount. The key difficulty arises from the need for assemble the components at room temperature, and

subsequently operate the camera at vacuum cryogenic temperatures. The different thermal expansion coefficients of the various materials considered for the lenslet mount drove the design requirements such that these components had to be held together with springs or flexures. The resulting arrangement is shown in Figure 3.

The lenslet array itself was made of low-Z silicon. Since the array was very thin (3 mm), a small amount of absorption was deemed acceptable. The lenslet array was fabricated with a gray-scale micro-optics process developed at WaveFront Sciences and then AR coated. Very precise dimensioning and tolerances were used to assure compatibility with the Titanium flexure. A thermal stress analysis of the flexure assembly confirmed that the lenslet array could be inserted with minimal force and remain stable at all operating temperatures. The gray scale fabrication process allowed up to four lenslets to be made simultaneously. The resulting design summary is given in Table 1.

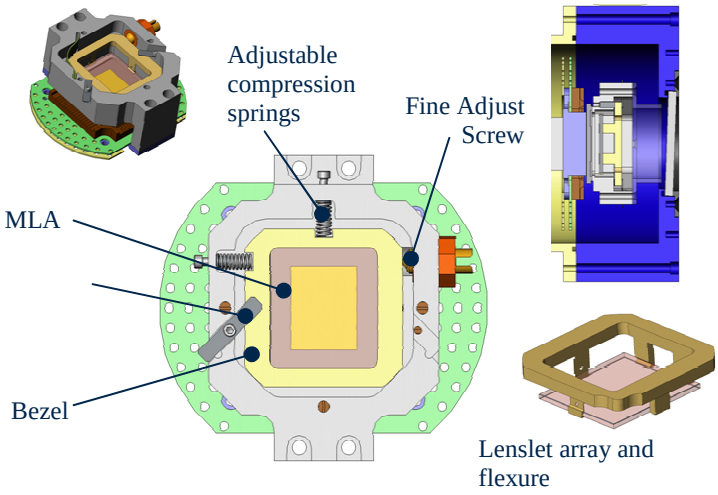

Figure 3 – Lenslet array mounting arrangement using Titanium flexures. The rotation is adjusted with a fine adjust screw through a removable vacuum feed-through on the side of the dewar body. The ZnSe input window is tilted slightly to minimize back-reflections.

5. Infra-Red Source Subsystem

The key requirement of the IR source system was to provide light at the correct wavelength that could be detected by the Phoenix camera as a point source to achieve the desired optical test geometry. To this end a CO_2 laser was selected at a wavelength of 9.271 microns. While the QWIP detector sensitivity rapidly decreases at this wavelength, sufficient responsivity was available considering the relatively high powers available from CO_2 lasers. In practice this turned out to pose some significant difficulties. The peak of the spectral sensitivity curve of the QWIP array is known only to within a tolerance of around +/- 0.1 microns. This makes it difficult to know the exact sensitivity of a given detector chip at the 9.271 µm wavelength and this number can vary significantly depending on the peak wavelength of the chip. Furthermore, even with active water cooled temperature control, we had difficulty achieving stable output power with a fixed cavity version of the Access Merit-G 2W laser. Ultimately we were able to operate the camera at a lower, but acceptable, S/N and eventually found a stable operating point for the laser.

Focal length	mm	**4.334**	3.456	3.255	5.567
Diameter	mm	**0.375**	0.375	0.325	0.425
Fresnel Number		**3.50**	4.39	3.50	3.50
Pixels/focal spot		**73**	47	55	94
Centroid accuracy	pixels	**0.012**	0.019	0.016	0.009
Predicted accuracy (zonal)	µm	**0.089**	0.175	0.147	0.057
Dynamic range	mr	**24.7**	35.7	28.5	21.8
Sag	µm	**3.35**	4.21	3.35	3.35
Number of levels		**32**	40	32	32

Table 1 WFS and lenslet array design summary. The first column represents the nominal design chosen. Note that LWIR wavefront sensors end up with a very large dynamic range, simply due to focal spot size considerations.

The CO_2 laser was mounted in an enclosure with a relay imaging system and focusing lens. The optical relay system could be adjusted to control the exit angle as shown in Figure 4. We used a diamond wire die as a pinhole. A visible diode laser was arranged so that it could be co-aligned with the IR beam for alignment purposes. To allow maximum flexibility in alignment all optics were made from ZnSe, which transmits both visible and IR. This source system was configured as a complete module with enclosure so that it could be positioned as a unit to allow for measurement of segments with different off-axis prescriptions. For the JWST program there are three positions (A, B, C). The geometry is shown in Figure 5.

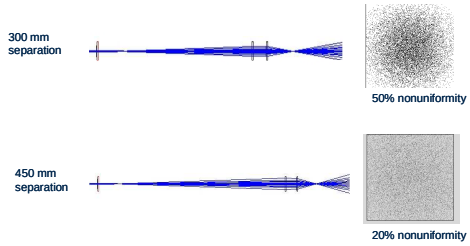

Figure 4 – Uniformity calculations of the source system through a pinhole. With the added relay lenses the system could be adjusted to control the final uniformity of the beam.

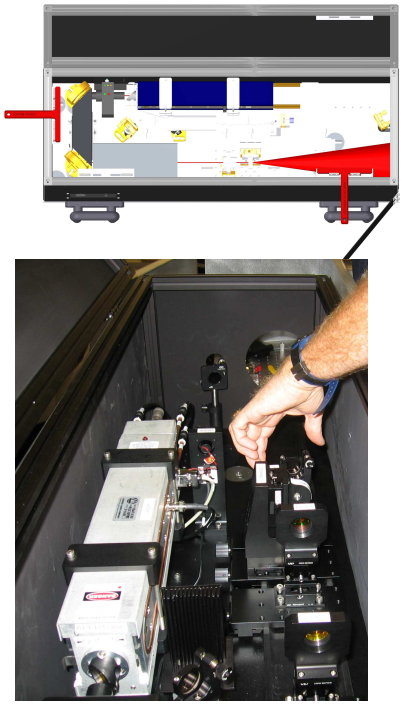

Figure 5 – Photograph of source system with CO2 laser and relay optics

6. The Scanning Paragon Gantry

An important element to the overall system design was the mechanical scanning system. This system had to support the WFS and telescope, and yet accurately scan over the full surface of the mirror, while maintaining precise pointing accuracy of the camera and telescope. Furthermore it could not obscure the beam during the measurement. This meant that the closest position of the end of the collecting optics was 1.1 m. This long optical path length lead to a tight requirement on the angular stability of the system, since any angular error would lead to an ambiguity in the measurement position. Since we wanted to be able to overlap adjacent regions accurate to $1/10^{th}$ lenslet, this led to a <50 μr pointing accuracy requirement of the gantry.

To meet these requirements, a custom air-bearing stage with linear motors was selected. Accurate encoders were used with closed loop control of all axes. The system was built and installed by Bell-Everman Corp. and met all performance specifications. A photograph of the gantry with the telescope and WFS installed is shown in Figure 6.

7. The Compressor Telescope

One key element of the system is a telescope to collect the light reflected from the mirror segment and image it onto the lenslet array of the WFS. The magnification of this telescope was chosen to give 1 mm resolution at the mirror surface which resulted in a 2.67:1 reduction. It is a Keplerian afocal design with aspheric Germanium lenses (focal length 494 and 185 mm) made by Light Works Optics, Inc. This telecentric telescope was arranged with shifted object/image planes so that the object distance was 1100 mm from the input lens with the image 100 mm from the output lens.

The telescope was integrated into an optomechanical assembly that also included mounting for the LWIR WFS. The entire system was arranged with a gimbal about the nodal point of the input lens and screw type mechanical adjustments for alignment. The WFS was also mounted on an adjustable platform providing tip and tilt adjustment that pivoted about the lenslet plane. The WFS position relative to the output lens was adjustable as was the output lens position (to collimate the telescope). The compressor telescope is shown in Figure 7

This arrangement facilitated the alignment of the system. The visible diode laser from the source system was first aligned from the center of the reference mirror to be parallel to the system optical axis. The gantry was used to position the laser at the entrance of the input lens. Then the CT was adjusted to center about the output lens. The WFS was then

adjusted to retro-reflect the beam back on itself. Once the visible (coarse) alignment was complete, the IR beam was used for final alignment using average tip tilt and centering information from the WFS. Perpendicularity and centering were also checked using this method.

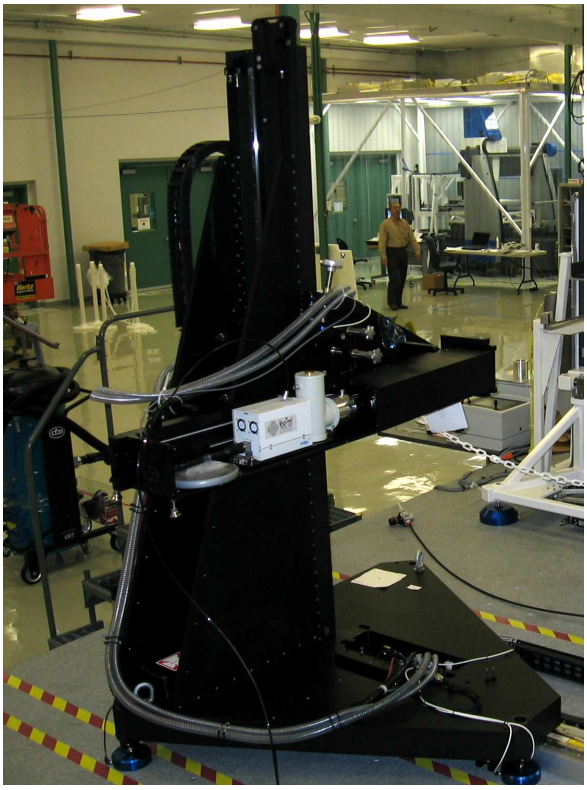

Figure 6 – Photograph of paragon gantry

8. The Reference Wave Front Subsystem

The reference wavefront system was used to provide an optical beam of known quality and known tilt for calibration. It was a gold coated, flat mirror, mounted in a computer controlled 2-axis mount with precision encoders. This allowed us to adjust the mirror to align the system and then record these positions for future reference. Furthermore, the mirror could be adjusted in small steps of tip or tilt and then measured on the wavefront sensor. This allowed calibration of the telescope magnification, lenslet focal length, and identification of optical errors in the system.

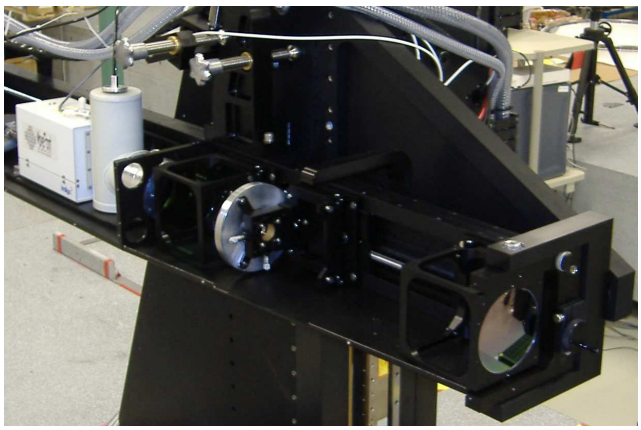

Figure 7 – Photograph of compressor telescope

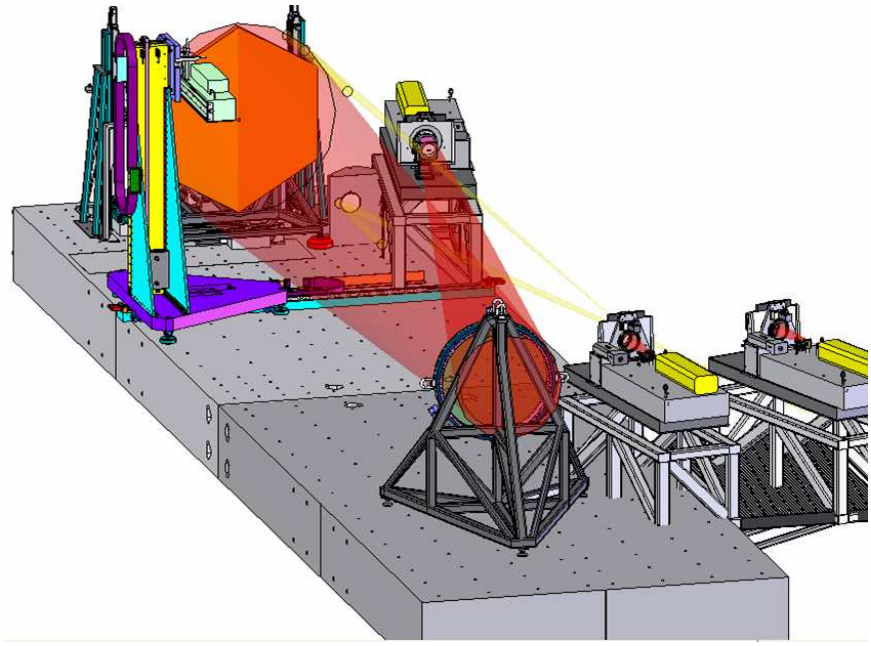

Figure 8 – Layout of SSHS system on granite block

9. SSHS System

A photograph of the completed system is shown in Figure 8. The system was assembled in a temperature controlled room on a large granite table.

1.3. Calibration

Two essential parameters need to be precisely calibrated for this system: telescope magnification and lenslet array focal length. To perform these calibrations we first precisely calibrate the paragon gantry using a distance measuring interferometer and the reference mirror using laser ray deflectometry. The magnification was calibrated by putting a small mask on the center of the reference mirror and then

using the gantry to move the mirror in known steps. The WFS data was analyzed to find the center of this irradiance pattern. The movement of the position of the pattern in camera space was compared to the gantry movement to obtain a precise estimate of the telescope magnification.

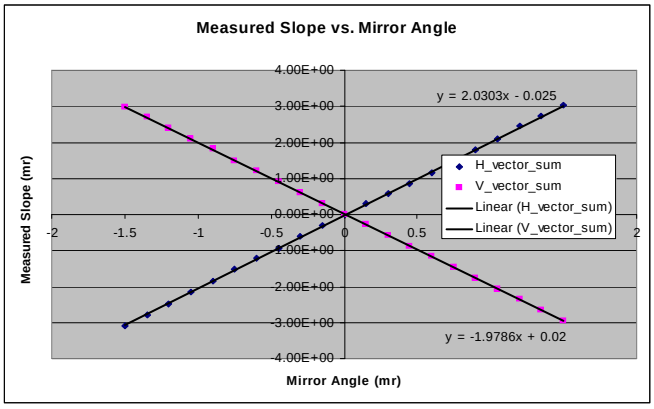

Figure 9– Calibration of the SSHS system (a) calibration of magnification (b) calibration of lenslet array focal length

To calibrate the lenslet focal length we used the reference mirror to introduce tilt in a known way. With the magnification from the previous step included in the analysis, the slope of the calibration curve now determined the lenslet array focal length (Figure 9b). For each mr of tilt introduced by the reference mirror, the calibrated system should measure a corresponding slope of 2 mr.

1.4. Measurement process

To measure a mirror segment, the gantry was positioned at the center of the mirror. Then the wavefront sensor average tip and tilt data was used to adjust the position of the mirror in x, y, θ_x and θ_y to reflect the source system light down the optical axis. The system software was designed to allow different measurement patterns with adjustable stitching overlaps. Our goal was to use 50% overlap on each measurement field since this results in averaging four measurements for each measurement points. In practice the computation time has limited us to slightly less than this. (optional Figure 11 showing stitching scan screen)

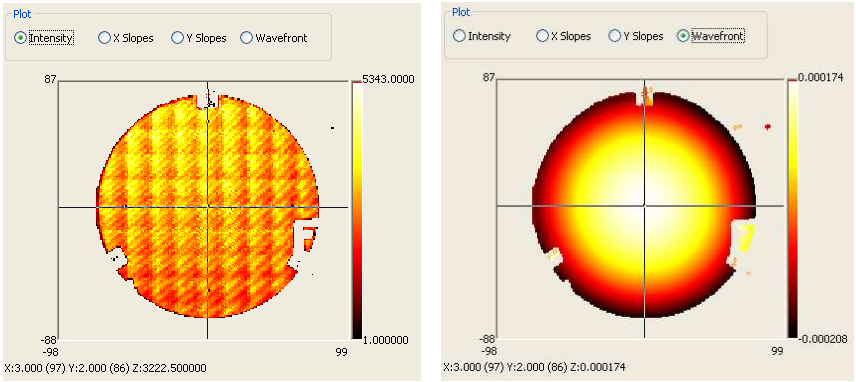

Figure 10– Stitched measurement from the reference mirror (a) full measurement, (b) measurement showing the tilt and focus subtracted

Figure 10 shows results from measuring the reference mirror and stitching the data. As can be seen there are not artifacts from the stitching of the data. While the point source reflecting from a flat mirror resulted in rays that exceed the design dynamic range, the system still produce good measurements but with reduced accuracy, even to the boundaries of the mirror.

10. SSHS Measurement Results

The key goal of this system is to measure Be mirrors in the rough ground state. To this end we tested the system (early in the program development) with a sample of Be with different grind patterns. An example image of the focal spot created by one lenslet is shown in Figure 12. The typical spot is clearly evident, with good Strehl and reasonable signal to noise ratio. In fact, we have been able to measure rougher sections of the Be mirror than originally anticipated

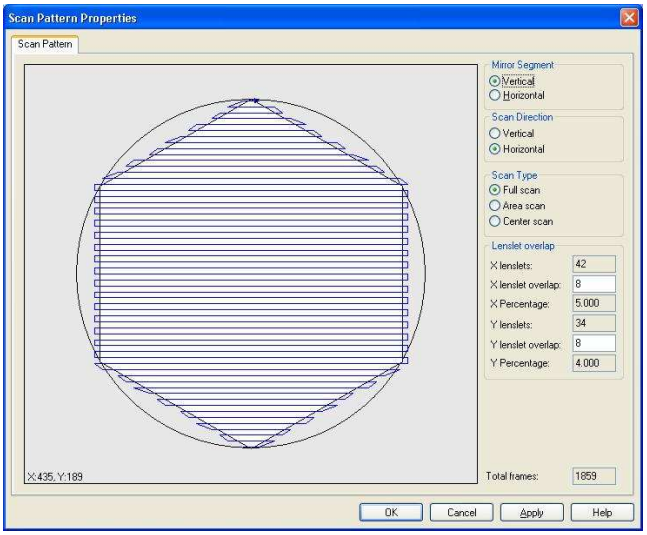

Figure 11 – SSHS software setup with different overlaps

1.5. Al surrogate

To validate the SSHS system, we used a number test articles that could be independently tested with CMM mechanical profilometry (Leitz PMM-C 24.16.7/B4). These included a large Aluminum surrogate mirror that was the same size and shape as the expected flight articles, but with a spherical curvature of radius. The surface finish of this segment was initially just machined aluminum. While we were able to get reasonable measurements over most of the surface, the focal spot Strehl ratio was poor and there were some areas where the surface was so rough that no data could be obtained. To ameliorate this, the surface was sanded using automotive body shop sanding methods and 320 grit sand paper. This resulted in a smooth enough surface that good measurements could be obtained over the whole surface. An example measurement is shown in Figure 13. Evident in this figure are residual lathe turning marks from the machining of the part.

11. SSHS Measurements Comparison to CMM measurements

One of the potential flight mirror segments, a test unit called the Engineering Development Unit (EDU) was measured on the SSHS system with additional CMM measurements to allow detailed validation of the measured accuracy. In Figure 17 the wavefront slopes in x and y and intensity and wavefront maps are presented. In the intensity map it is evident that there are some regions that have different reflectivity. These are evident looking at the mirror as these are regions that have not yet been figured.

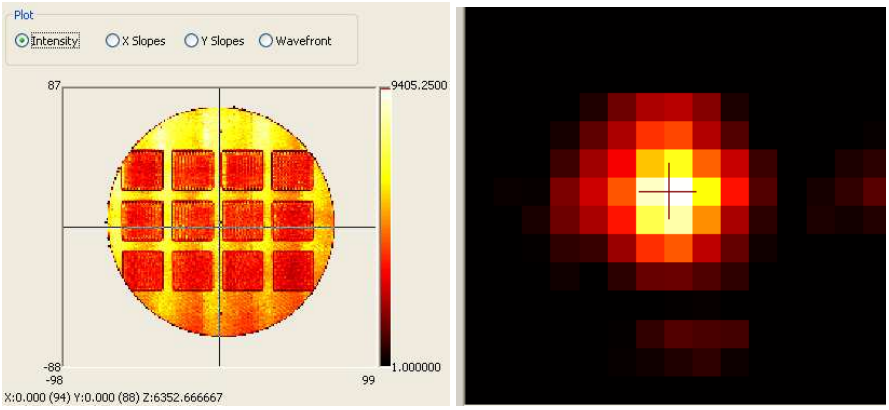

(a) (b)

Figure 12–(a) Measured sample patches of different grind samples on a Be substrate. (b) Single measured focal spot from light reflected from a Be sample with rough grind.

The wavefront shows a large amount of residual astigmatism, which may be partly due to just the test configuration. If we subtract this astigmatism and other terms (based on Zernike notation), then the underlying structure becomes much more apparent. Figure 14 shows a circular masked region of the center 1200 mm of the EDU with Zernike terms through 5th order subtracted. In this figure the print through from the back surface support structure (a triangular pattern) is clearly evident.

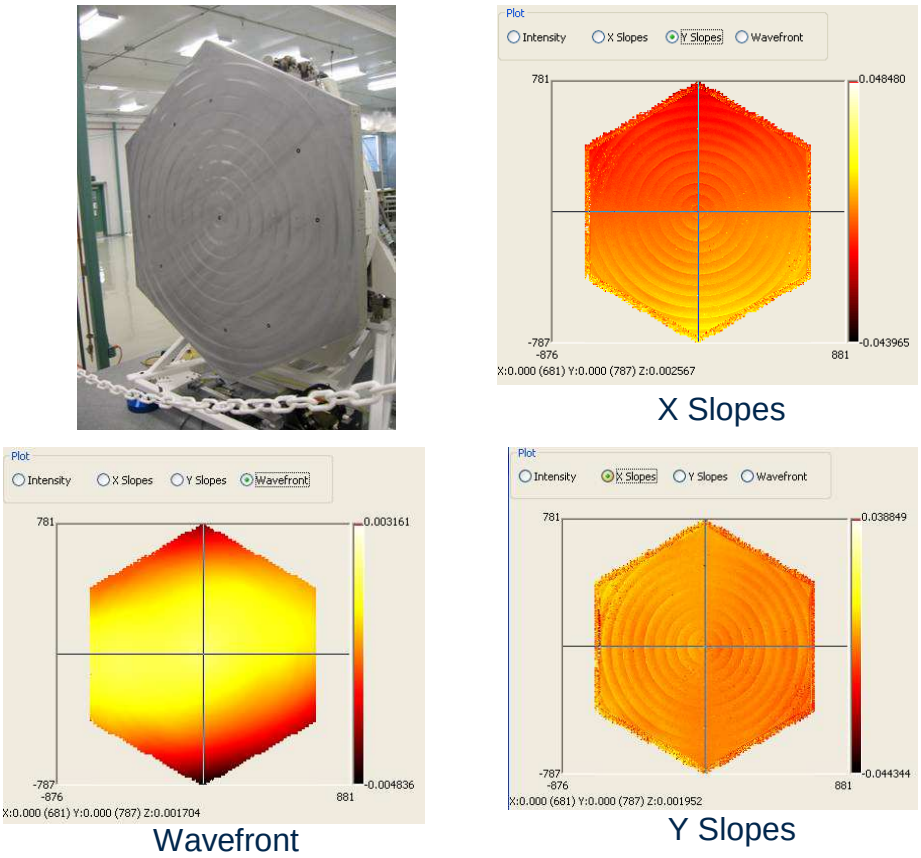

Figure 13 – Measurement of the Aluminum surrogate mirror. The fabrication rings can be clearly seen in the x and y slope maps. These features are present in the wavefront map as well, but are difficult to see because of the larger low order terms. Edge effects controls have not yet been implemented (see Fig. 17)

As a final validation, we compared the SSHS data with the CMM. This is presented in Figure 15. Both of these data sets have been filtered to remove the low order spatial frequency terms. The CMM data was taken in drag probe mode in nested hexagonal scan lines with variable line spacing of 1 mm near the edge to 10 mm at part center, which took 36 hours to acquire, whereas the SSHS data was acquired in about 35 min. In the comparison the same features are evident in both pictures, although it is difficult to get a sense of exact correspondence because of plot auto-scaling. Furthermore, the mirror segment is measured horizontally in the CMM and vertically in the SSHS. While this mirror is very light (~40 lbs) due to its Be construction, there is still some mounting effect that must be taken into consideration.

The comparison can be seen better in a line profile from each data set. Figure 16 shows such a profile with both data sets superimposed. Clearly the two measurements track each other well with < 5 um total variation. The overall difference between the two lines is <1 um RMS. Some experiments with repeatability on the CMM indicate that over these large areas there may be up to 5 um P-V error in the CMM data, so this is probably as good a match between the two data sets that can be expected. Other experiments with smoother optics tested over smaller regions have indicated that the SSHS system is meeting its goal of <1 um PV overall accuracy.

12. Summary and Conclusions

This paper reports on the development of a new metrology testing system for testing large optics mirrors early in the fabrication process. The system has a number of innovative components:

- A long wavelength Infrared Shack-Hartmann based wavefront sensor that allows measurement of rough grind surfaces. Thus the mirror segment can be measured at any point in the fabrication sequence and there is no need to do any figuring or polishing just for metrology.

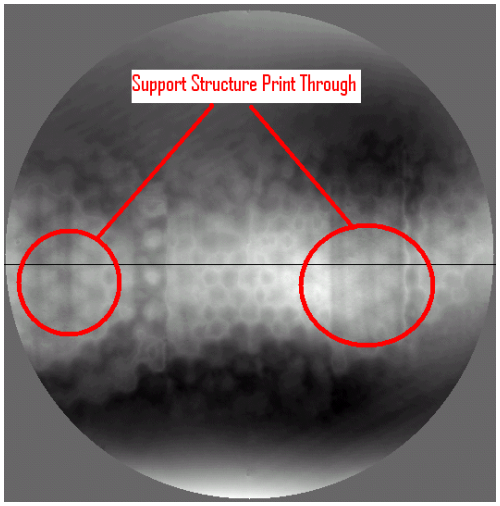

Figure 14 Masked section of the EDU wavefront data

- A scanning and stitching metrology system that is scalable to all different size mirrors. Larger mirrors would only require a larger gantry or a different test configuration.
- Testing from point sources at prime focus so that no null lenses or other special test optics are needed.
- Extremely large dynamic range sensor so that very rapid variations in surface slope can be accurately measured, even to within a few mm of the edge.

This system is already installed and has just finished system validation for testing the JWST mirror segments. A second system is starting system integration. These two systems are expected to be in constant use during the grinding and polishing of the 18 JWST segments over the next few years.

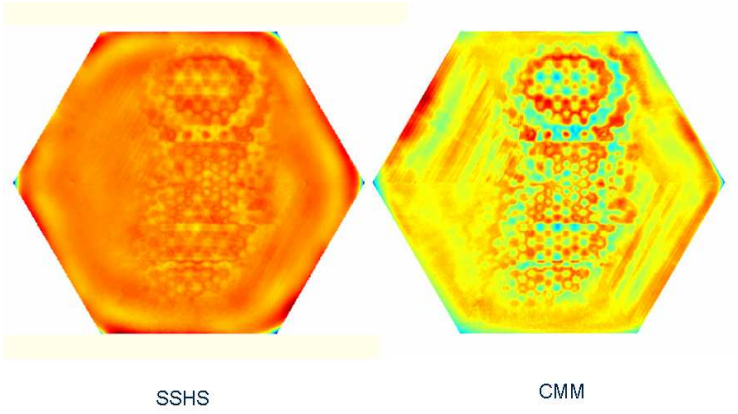

Figure 15 Comparison of SSH sand CMM surface maps after filtering the data to remove the low spatial frequency components

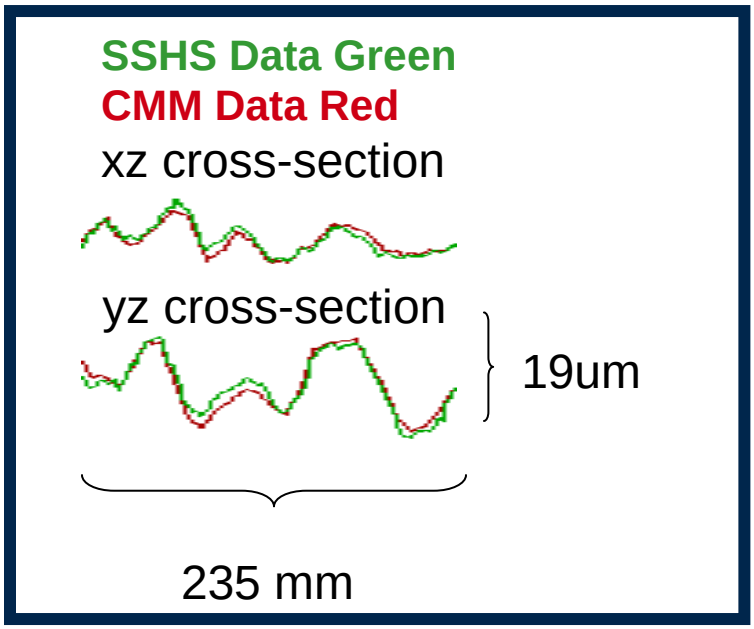

Figure 16 Comparison of SSH sand CMM cross sections

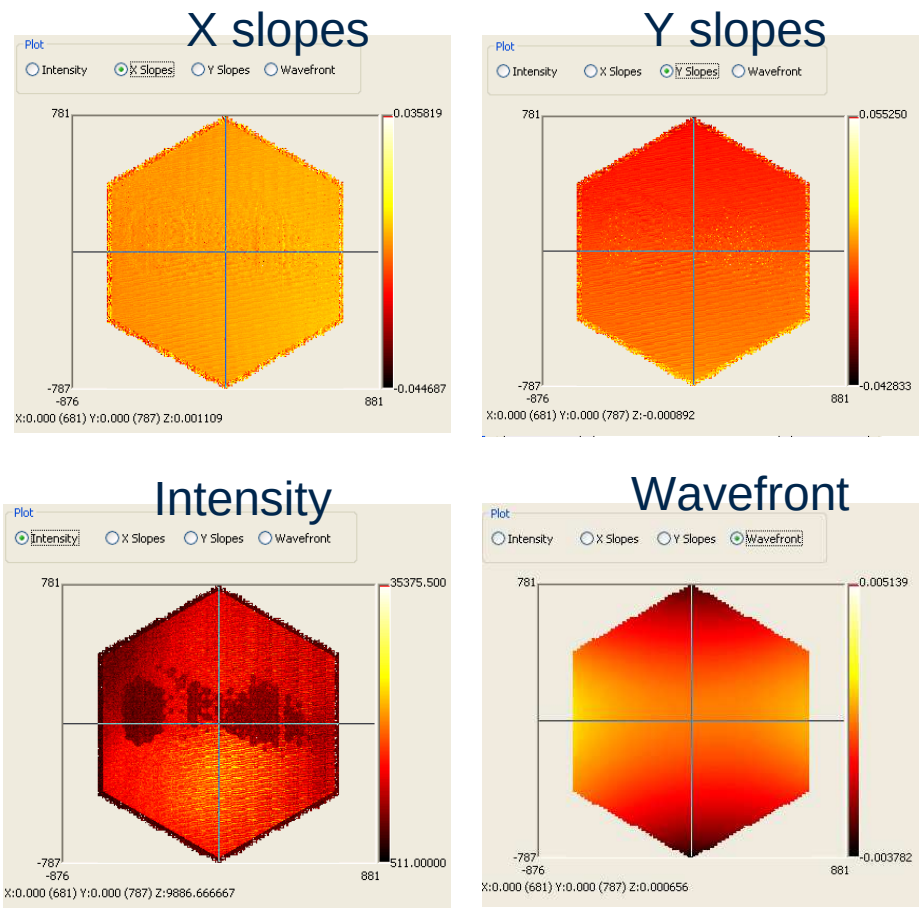

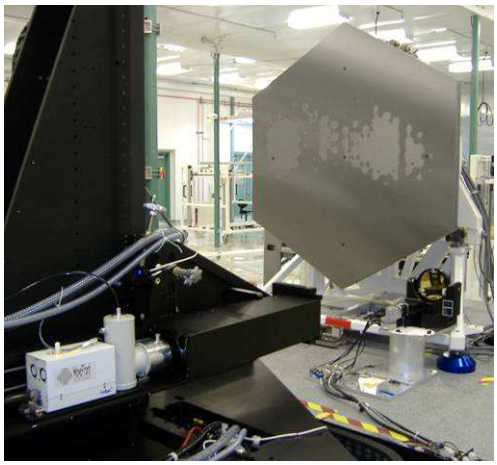

Figure 17 – Measurement of the EDU with the SSHS system. Note that the edges appear ragged due to room background. The intensity map shows the edges clearly and is used to define a mask to clean up the edges.

[1] 1 G. C. Cole, T. Peters, K. W. Johnson, W. Wolff, R. S. Garfield, T. Nassar, H. A. Wong, R. J. Bernier, C. D. Kiikka, J. M. Kincade, T. B. Hull, Tinsley Labs.; B. B. Gallagher, D. M. Chaney, R. J. Brown, Ball Aerospace & Technologies Corp.; A. G. McKay, Northrop Grumman Space Technology, "An overview of optical fabrication of the JWST mirror segments at Tinsley," *SPIE* **6265**-29.

[2] R. Bernier, G. C. Cole, C. R. Alongi, T. Peters, J. M. Kincade, T. B. Hull, Tinsley Labs.; B. B. Gallagher, Ball Aerospace & Technologies Corp.; A. G. McKay, Northrop Grumman Space Technology, "A system of metrology for the JWST mirror segments at Tinsley," *SPIE* **6265** -123.

[3] T.D. Raymond, D.R. Neal, D.M. Topa, and T.L. Schmitz, "High-speed, non-interferometric nanotopographic characterization of Si wafer surfaces," *SPIE* **4809**-34, 2002.
[4] D. R. Neal, "Shack-Hartmann sensor engineered for commercial measurement applications," *SPIE* **AM100-20** (2004).
[5] J. Schwiegerling and D. R. Neal, "Historical Development of the Shack-Hartmann Wavefront Sensor," *SPIE* **AM100-19** (2004).
[6] D. R. Neal, J. Copland, D.A. Neal, "Shack-Hartmann wavefront sensor precision and accuracy," *SPIE* **4779**, 2002.
[7] D. R. Neal, D. J Armstrong, W. T. Turner, "Characterization of Infrared Laser Systems," *SPIE* **3437**-05 (1998).
[8] D. R. Neal, P. Pulaski, T.D. Raymond, and D. A. Neal, "Testing highly aberrated large optics with a Shack-Hartmann wavefront sensor," *SPIE* **5162**, 2003.

[9] D. R. Neal, D. J. Armstrong and W. T. Turner, "Wavefront sensors for control and process monitoring in optics manufacture," *SPIE* **2993**, pp. 211–220, 1997.